












RESEARCH ARTICLE

Associations of white matter hyperintensities with networks of gray matter blood flow and volume in midlife adults: A coronary artery risk development in young adults magnetic resonance imaging substudy

William S. H. Kim^{1,2}  | Nicholas J. Luciw^{1,2}  | Sarah Atwi^{1,2}  | Zahra Shirzadi^{1,2}  |
 Sudipto Dolui^{3,4,5}  | John A. Detre^{3,4,5}  | Ilya M. Nasrallah⁵  |
 Walter Swardfager^{2,6,7,8,9}  | Robert Nick Bryan¹⁰  | Lenore J. Launer¹¹  |
 Bradley J. MacIntosh^{1,2,6,9} 

¹Department of Medical Biophysics, University of Toronto, Toronto, Ontario, Canada

²Hurvitz Brain Sciences Program, Sunnybrook Research Institute, Toronto, Ontario, Canada

³Center for Functional Neuroimaging, University of Pennsylvania, Philadelphia, Pennsylvania, USA

⁴Department of Neurology, University of Pennsylvania, Philadelphia, Pennsylvania, USA

⁵Department of Radiology, University of Pennsylvania, Philadelphia, Pennsylvania, USA

⁶Canadian Partnership for Stroke Recovery, Sunnybrook Research Institute, Toronto, Ontario, Canada

⁷Department of Pharmacology and Toxicology, University of Toronto, Toronto, Ontario, Canada

⁸Toronto Rehabilitation Institute, University Health Network, Toronto, Ontario, Canada

⁹Dr. Sandra Black Centre for Brain Resilience & Recovery, Sunnybrook Research Institute, Toronto, Ontario, Canada

¹⁰Department of Diagnostic Medicine, University of Texas, Austin, Texas, USA

¹¹Laboratory of Epidemiology and Population Science, National Institute on Aging, Bethesda, Maryland, USA

Correspondence

Bradley J. MacIntosh, Sunnybrook Research Institute, University of Toronto, 2075 Bayview Ave, Room M6-180, Toronto, ON M4N 3M5, Canada.

Email: brad.macintosh@utoronto.ca

Abstract

White matter hyperintensities (WMHs) are emblematic of cerebral small vessel disease, yet effects on the brain have not been well characterized at midlife. Here, we investigated whether WMH volume is associated with brain network alterations in midlife adults. Two hundred and fifty-four participants from the Coronary Artery Risk Development in Young Adults study were selected and stratified by WMH burden into Lo-WMH (mean age = 50 ± 3.5 years) and Hi-WMH (mean age = 51 ± 3.7 years) groups of equal size. We constructed group-level covariance networks based on cerebral blood flow (CBF) and gray matter volume (GMV) maps across 74 gray matter regions. Through consensus clustering, we found that both CBF and GMV covariance networks partitioned into modules that were largely consistent between groups. Next, CBF and GMV covariance network topologies were compared between Lo- and Hi-WMH groups at global (clustering coefficient, characteristic path length, global efficiency) and regional (degree, betweenness centrality, local efficiency) levels. At the global level, there were no between-group differences in either CBF or GMV covariance networks. In contrast, we found between-group differences in the regional degree, betweenness centrality, and local efficiency of several brain regions in both CBF and GMV covariance networks. Overall, CBF and GMV covariance analyses provide evidence that WMH-related network alterations are present at midlife.

KEYWORDS

CARDIA, cerebral blood flow, covariance, graph theory, gray matter volume, small vessel disease, white matter hyperintensities

This is an open access article under the terms of the [Creative Commons Attribution-NonCommercial-NoDerivs](https://creativecommons.org/licenses/by-nc-nd/4.0/) License, which permits use and distribution in any medium, provided the original work is properly cited, the use is non-commercial and no modifications or adaptations are made.

© 2022 The Authors. *Human Brain Mapping* published by Wiley Periodicals LLC.

Funding information

Brain and Behavior Research Foundation; Canadian Institutes of Health Research, Grant/Award Number: 165981; National Heart, Lung, and Blood Institute, Grant/Award Numbers: HHSN268201800003I, HHSN268201800004I, HHSN268201800005I, HHSN268201800006I, HHSN268201800007I; National Institute on Aging, Grant/Award Number: AG0005

1 | INTRODUCTION

White matter hyperintensities (WMHs) of presumed vascular origin are one of the most widely studied markers of cerebral small vessel disease (SVD) (Wardlaw et al., 2019) and are associated with vascular risk factors (De Leeuw et al., 1999), cognitive decline (De Groot et al., 2001), gait abnormalities (Baezner et al., 2008; De Laat et al., 2011), depression (Rabins et al., 1991), and brain atrophy in late-life individuals (Appelman et al., 2009; Godin et al., 2009; Rossi et al., 2006; Schmidt et al., 2005). Whereas WMHs have been well studied in late-life, comparatively less is known regarding their effects on brain function in earlier adult decades of life (Cannistraro et al., 2019). Notably, WMHs are present in midlife (i.e., forties, fifties) (Bryan et al., 1999; Launer et al., 2015; Medley, 1980; Wen et al., 2009) and are associated with an increased risk of late-life dementia and early cognitive impairment (d'Arbeloff et al., 2019; Smith et al., 2015).

The mechanisms by which WMHs affect the brain are not fully established, however one potential consequence is the alteration of brain networks (Lawrence et al., 2014). As articulated in a recent review, focal WMHs can impact remote brain regions and structural and functional network connections (Ter Telgte et al., 2018). Multivariate methods that integrate information across brain regions may help elucidate the widespread consequences of WMHs beyond conventional neuroimaging biomarker research (Wee et al., 2013). SVD has been viewed predominantly as affecting subcortical anatomy proximal to focal lesions, including white matter as well as thalamic and basal ganglia regions (Wardlaw et al., 2013). However, these regions may represent only a fraction of SVD-related consequences across the brain. Covariance analysis of neuroimaging data is one such multivariate approach that can be used to infer network-like associations between brain regions. This technique exploits the phenomenon of inter-regional covariation between properties of select brain regions across a population sample (Alexander-Bloch, Giedd, & Bullmore, 2013; Melie-García et al., 2013). Typically, covariance analysis involves the construction of group-level networks based upon the pairwise correlation of regional measures of structure, such as gray matter volume (GMV) or cortical thickness. These structural covariance networks are thought to arise from various intrinsic factors, such as coordinated morphological change throughout development or synchronized maturation due to mutually trophic influences, as well as extrinsic factors such as common effects of risk factors and other pathology (Alexander-Bloch, Giedd, & Bullmore, 2013; Alexander-Bloch, Raznahan, et al., 2013). Structural covariance networks only

partially resemble networks derived from white matter tractography or functional connectivity and therefore seem to probe unique organizational aspects of the brain (Gong et al., 2012; Kelly et al., 2012).

There is a need for multimodal structural and functional neuroimaging studies to elucidate the mechanisms by which SVD might lead to clinical deficits, especially in earlier adult decades of life (Ter Telgte et al., 2018). Cerebral blood flow (CBF) is an important and dynamic measure of brain health and metabolism that is subject to regional and global physiological fluctuations at varying timescales. At the group-level, CBF covariance captures stable relationships of inter-regional CBF across participants. Several biological factors are thought to affect CBF covariance, including synchronized neuronal activity via neurovascular coupling, structural connectivity, and shared vascular supply (Luciw et al., 2021; Melie-García et al., 2013). Importantly, structural covariance networks and covariance networks derived from CBF (as well as other physiological neuroimaging contrasts, such as glucose metabolism) exhibit significant yet modest correspondence, suggesting that they provide complementary but distinct information (Di et al., 2017; Luciw et al., 2021). Therefore, given that CBF covariance can provide metabolic and vascular information, it is important to consider this imaging contrast alongside structural covariance (Luciw et al., 2021; Melie-García et al., 2013).

Graph theory is a mathematical framework that can be used to characterize covariance networks and has played a crucial role in establishing the brain as an efficient and sparsely connected “small-world” network (Alexander-Bloch, Giedd, & Bullmore, 2013). Considering the brain as a set of nodes (i.e., brain regions) and edges (i.e., connections between nodes, such as pairwise correlations), graph theory produces a number of properties that describe the global and regional topologies of brain networks (Box 1; Rubinov & Sporns, 2010). In healthy adults, both CBF and GMV covariance networks have been found to exhibit small-world properties when compared to simulated networks in which edges are drawn at random between nodes (Alexander-Bloch, Raznahan, et al., 2013; Melie-García et al., 2013). Therefore, network properties derived from graph theory may provide insight into disease-related changes of such covariance networks (Alexander-Bloch, Giedd, & Bullmore, 2013). Indeed, within the larger context of SVD, the application of graph theory has pointed to anomalous structural (Frey et al., 2020; Lawrence et al., 2014; Reijmer et al., 2016; Tuladhar et al., 2016, 2017), functional (Chen et al., 2019; Sang et al., 2018; Schaefer et al., 2014), and structural covariance network efficiency (Nestor et al., 2017; Tuladhar et al., 2015), albeit typically in older populations. For instance, one study found that higher WMH volume was linked to a higher clustering coefficient (a measure of

BOX 1 Graph theoretical properties of global and regional network topology investigated in this study

Global network properties, such as the clustering coefficient (average of the fraction of a node's neighbors that are neighbors of each other across all nodes), characteristic path length (average shortest path length in the network), and global efficiency (average inverse shortest path length in the network) reflect network-wide attributes. Regional network properties, such as the degree (number of edges on a node), betweenness centrality (measure of the number of shortest paths that travel through a given node), and local efficiency (measure of efficiency in a node's set of neighbors upon its removal) describe the contribution of individual brain regions that enable efficient communication throughout the network.

network segregation) in structural covariance networks derived from cortical thickness; the authors of this study posit that this may be due to coordinated thinning of the cortex rather than increase in local connectivity (Tuladhar et al., 2015). Moreover, by considering several global and regional network properties, a fuller understanding of the network can be surmised.

This study investigates CBF and GMV covariance networks in midlife adults from the Coronary Artery Risk Development in Young Adults (CARDIA) study. A subset of participants from the 25-year CARDIA brain MRI study were stratified by WMH burden into two groups. CBF and GMV covariance networks were generated for each group and compared using graph theoretical properties of global and regional network topology. We hypothesize that it will be possible to identify differences in CBF and GMV covariance network topology among midlife adults with higher WMH volume when compared against a control group with lower WMH volume. SVD is thought to lead to disruption of brain networks; this disruption may arise from combined topological changes of the network at global and regional scales. Therefore, this study was exploratory with respect to the directionality of effects on the considered graph theoretical properties.

2 | METHODS

2.1 | Participants

The CARDIA study is a longitudinal multi-site prospective study aiming to investigate the evolution of cardiovascular disease over adulthood. Participants were initially recruited in 1985 and between 18 and 30 years of age and provided written informed consent at each exam. Institutional review boards from each CARDIA center and

the coordinating center (University of Minnesota Institutional Review Board, Kaiser-Permanente Northern California Institutional Review Board) approved this study annually. The present study uses brain MRI data from the 25-year follow-up exam (at which point participants were between 43 and 55 years of age) collected at two of four CARDIA centers in the United States (Minneapolis, MN and Oakland, CA).

Clinical measures obtained at the 25-year follow-up exam included: body mass index (BMI, from height and weight); diastolic and systolic blood pressure assessed using a digital blood pressure monitor (OmRON HEM-907XL; Online Fitness, CA); smoking status; diabetes diagnosis (American Diabetes Association, 2011); and blood samples provided estimates of concentrations of high- and low-density lipoprotein cholesterol and triglycerides.

2.2 | MRI acquisition

The MRI sequences for the current study were previously described (Launer et al., 2015), and consisted of T1-weighted, T2-weighted fluid-attenuated inversion recovery (FLAIR), and pseudo-continuous arterial spin labeling (ASL) imaging acquired on Siemens 3 Tesla Tim Trio MRI scanners. Isotropic T1-weighted images were acquired using a sagittal magnetization-prepared rapid gradient-echo sequence (TR/TE/TI = 1900/2.9/900 ms, spatial resolution = 1 mm³, FOV = 250 mm, slices = 176, flip angle = 90°, GRAPPA = 2, bandwidth = 170 Hz/pixel). Isotropic T2-weighted images were acquired using a sagittal FLAIR sequence (TR/TE/TI = 6000/285/2200 ms, spatial resolution = 1 mm³, FOV = 258 mm, slices = 160). CBF maps were calculated from ASL imaging acquired using pseudo-continuous labeling and a two-dimensional multi-slice gradient-echo planar imaging readout (TR/TE = 4000/11 ms, spatial resolution = 3.4 × 3.4 × 5 mm³, FOV = 220 mm, flip angle = 90, bandwidth = 3004 Hz/pixel, echo spacing = 0.44 ms, EPI factor = 64, label duration = 1.48 s, offset = 90 mm, radio-frequency pulse gap = 0.36 ms, pulse duration = 0.5 ms, mean z-direction gradient = 0.6 mT/m, post-label delay of 1500 ms [range of 1500 to 2170 ms from most inferior to superior slices], no background suppression, 40 control-label pairs).

2.3 | MRI processing

MRI data were processed using SPM8 (www.fil.ion.ucl.ac.uk/spm/software/spm8) and programs developed in MATLAB (MathWorks Inc.) and has been described previously (Launer et al., 2015). Structural images were processed using a previously described multimodal segmentation algorithm to classify tissue into gray matter (GM), white matter (WM), and cerebrospinal fluid (CSF) (Goldszal et al., 1998; Shen & Davatzikos, 2002). GM and WM were then assigned to 98 regions as defined by the Jakob atlas (Kabani et al., 1998). Of these, we chose the 74 regions classified as GM (see Table S1).

WMHs were segmented from structural images using a previously reported deep-learning classification model, built on the U-Net

TABLE 1 Demographic and clinical characteristics

	Lo-WMH (n = 127)	Hi-WMH (n = 127)	Test statistic	p
Age (years)	50 ± 3.5	51 ± 3.7	U = 6708.5	.01*
Female (%)	51 (40.0)	80 (63.0)	$\chi^2 = 12.36$	<.001*
Caucasian, n (%)	70 (55.1)	82 (64.6)	$\chi^2 = 1.98$.16
Smoking (%)	67 (52.8)	68 (53.5)	$\chi^2 = 0.00$	-
Diabetes (%)	3 (2.4)	1 (0.1)	$\chi^2 = 0.25$.61
MRI site (1/2)	63/64	68/59	$\chi^2 = 0.25$.62
BMI (kg/m ²)	29.1 ± 5.0	28.2 ± 5.3	U = 7052.5	.04*
DBP (mmHg)	74.1 ± 10.5	73.4 ± 11.1	U = 7768.0	.31
SBP (mmHg)	118.3 ± 12.7	117.8 ± 15.8	U = 7633.5	.23
HDL (mg/dl)	56.4 ± 17.0	60.7 ± 16.3	U = 6649.5	.008*
LDL (mg/dl)	116.7 ± 36.1	117.6 ± 30.2	U = 7579.0	.20
Triglycerides (mg/dl)	110.2 ± 60.9	102.7 ± 58.9	U = 7472.0	.16
Global CBF (ml/100 g/min)	56.1 ± 12.3	56.6 ± 11.2	U = 7818.0	.34
Global GMV (ml)	516.3 ± 55.3	521.5 ± 45.2	U = 7610.5	.44
ICV (ml)	1203.5 ± 138.4	1215.9 ± 114.2	U = 7671.0	.25
WMH (ml)	0.52 ± 0.22	2.87 ± 1.83	U = 0.0	<.001*

Note: Data are presented as mean ± standard deviation, or count (%). *p*-Values were calculated Mann-Whitney *U* tests for continuous variables and chi-squared tests for categorical variables. **p* < .05.

Abbreviations: BMI, body mass index; CBF, cerebral blood flow; DBP, diastolic blood pressure; GMV, gray matter volume; HDL, high-density lipoprotein; ICV, intracranial volume; LDL, low-density lipoprotein; MRI, magnetic resonance imaging; SBP, systolic blood pressure; WMH, white matter hyperintensity.

architecture and internal convolutional network Inception ResNet layers (Nasrallah, Pajewski, et al., 2019). The model was trained using a large and heterogeneous training set with human-validated WMH segmentations.

ASL time series data were first motion corrected, followed by regression of residual motion artifacts (Wang, 2012). A Gaussian smoothing kernel with full-width-half-maximum of 5 mm was used to spatially smooth images. A CBF time series was then obtained by pairwise control-label subtraction. CBF image intensities were converted to absolute units after averaging difference images and performing voxel-wise calibration using the ASL control image as the estimate of the equilibrium magnetization (Dolui et al., 2016). CBF maps were then linearly registered to T1-weighted images and mean regional CBF measures were obtained using the same 74 GM regions.

2.4 | Group stratification

Participants were selected from an available total sample of 421 for which processed data was fully available. Participants were stratified by WMH burden to create two groups for subsequent analyses (Figure 1). A nominal WMH volume was measured in all but a small number of participants; as such, we were not powered to stratify groups on the presence of WMH volume alone. Instead, WMH volumes were normalized by intracranial volume and log-transformed to normalize the skewed distribution. Participants in the 7th to 10th deciles of log-transformed WMH volume were denoted as the “Hi-

WMH” group (*n* = 127). For comparison, participants in the 1st to 3rd deciles of log-transformed WMH volume were taken to be the “Lo-WMH” group (*n* = 127). Although others have stratified groups based on a median split of WMH volume (Mahinrad et al., 2020), our sample was large enough to omit the 4th to 6th deciles and thereby ensure a clear delineation between the two groups.

2.5 | Network analysis

Network analysis was performed in Python 3.7.6 (www.python.org/downloads/release/python-376/) using the Brain Connectivity Toolbox package (www.pypi.org/project/bctpy/) (Rubinov & Sporns, 2010). CBF and GMV measures were first intensity normalized (i.e., divided by global CBF or GMV) on a per participant basis. Across all participants in both Lo- and Hi-WMH groups, normalized CBF and GMV measures were then adjusted on a per region basis using a linear regression model by removing the variance attributed to the following variables: age, sex, race, BMI, and MRI site. Note that we purposefully chose to exclude global CBF and GMV as covariates to maintain consistency between CBF and GMV analyses. The adjusted measures were then used to calculate Pearson's correlation coefficients between all brain region pairs, resulting in 74 × 74 covariance matrices. This procedure was performed for both Lo- and Hi-WMH groups, resulting in a total of four covariance matrices (i.e., two matrices × two groups). Diagonal matrix elements, representing self-connections, were excluded.

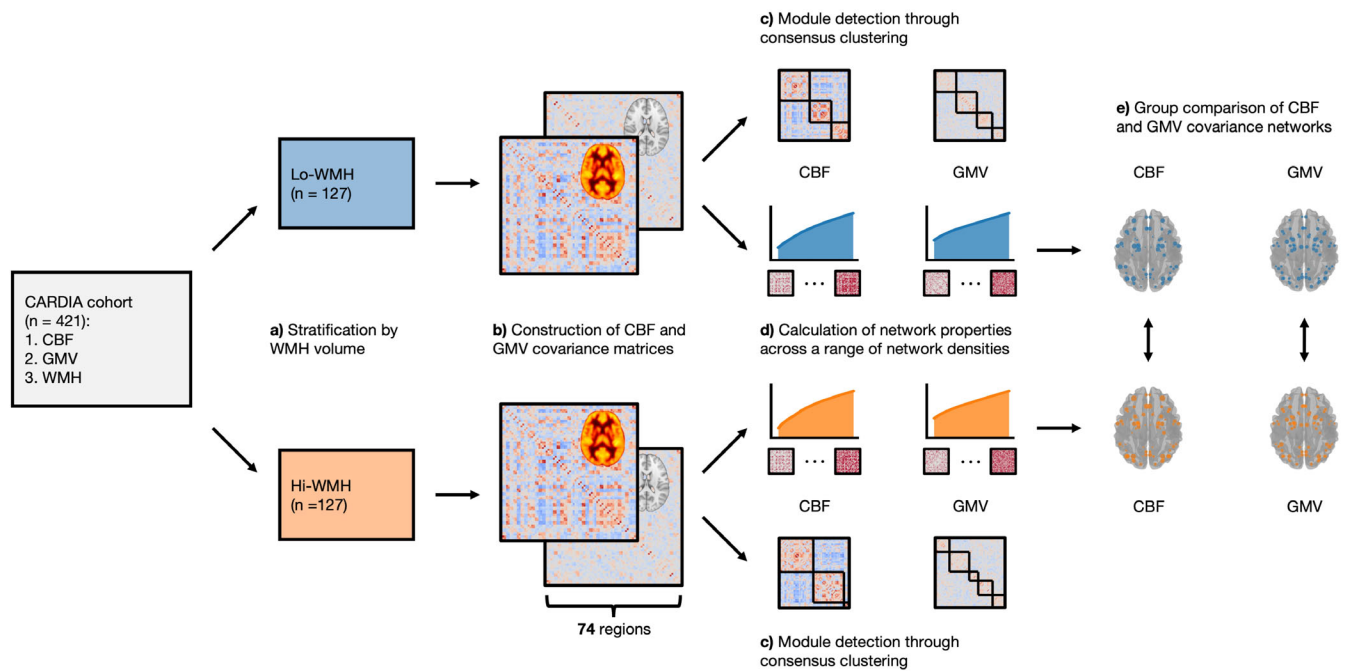


FIGURE 1 Illustration of analytic workflow. (a) Participants were stratified by white matter hyperintensities (WMH) volume into two groups. (b) Group covariance matrices were constructed from cerebral blood flow (CBF) and gray matter volume (GMV) data by Pearson's correlation coefficient between all brain region pairs, adjusted for age, sex, body mass index, race, and magnetic resonance imaging site. (c) Consensus clustering was performed to detect modules from CBF and GMV covariance matrices. (d) Network properties were calculated from CBF and GMV covariance matrices across a range of network densities and area-under-the-curve was integrated to summarize network properties. (e) CBF and GMV covariance networks were compared between Lo- and Hi-WMH groups at global (clustering coefficient, characteristic path length, global efficiency) and regional (degree, betweenness centrality, local efficiency) levels using a nonparametric procedure

We deployed a community detection analysis on the covariance matrices to partition the 74 brain regions into modules (i.e., clusters) with high internal covariance. Briefly, covariance matrices underwent 100 iterations of the Louvain community detection algorithm at selected resolution parameter values of 1.25 for CBF covariance matrices and 0.75 for GMV covariance matrices (see Supporting Information S1; Blondel et al., 2008). Across all iterations, we calculated the probability that a brain region pair was consistently assigned to the same module, yielding a 74×74 agreement matrix, which was then thresholded at 0.5 (Cohen & D'Esposito, 2016). Finally, we performed consensus clustering on the agreement matrix using the Louvain algorithm with 100 iterations, yielding a single consensus modular partition (Lancichinetti & Fortunato, 2012). Unlike conventional clustering approaches, this analytic framework defines the number of modules from the data. To quantify the similarity of partitions between Lo- and Hi-WMH groups, we calculated the Hamming distance between their modular partitions.

To characterize network topology, covariance matrices were thresholded and binarized across a range of network densities (0.16 to 0.50, increments of 0.01). The density of a matrix is defined as the number of non-zero edges divided by the total possible number of edges (i.e., $[74 \times 73]/2$). The minimum network density was chosen such that all brain regions had at least one non-zero edge (i.e., connected to at least one other region within the network). At each of these network densities, we calculated global (clustering coefficient, characteristic path length, and global efficiency) and

regional (degree, betweenness centrality, and local efficiency) graph theoretical properties to characterize network topology (Box 1). Across the range of network densities, global and regional network properties were summarized by the area-under-the-curve (Figure 1).

Finally, we computed the small-world coefficient across the range of network densities, defined as the ratio between normalized clustering coefficient and normalized characteristic path length (i.e., normalized by 100 random networks that preserve the number of nodes and edges as well as the degree of individual nodes). Networks with a small-world coefficient greater than 1 are thought to maximize efficiency of information transfer while minimizing "wiring costs," thus providing a balance between functional segregation and integration (Watts & Strogatz, 1998).

2.6 | Statistical analysis

Demographic and clinical characteristics were compared between groups using Mann-Whitney *U* tests for continuous variables and chi-squared tests for categorical variables.

To compare network properties between Lo- and Hi-WMH groups, we used a nonparametric permutation approach with 10,000 permutations. With each permutation, participants were shuffled into two randomized groups of equal size ($n = 127$, each). CBF and GMV covariance matrices were re-constructed, modular partitions were re-

generated, network properties were re-calculated across the range of network densities, and area-under-the-curve was re-integrated. Differences in network modular partitions and network properties between the two randomized groups were used to create null distributions. The observed differences between Lo- and Hi-WMH groups was then compared against the corresponding null distributions, resulting in nonparametric p -values derived as the relative position of the observed difference compared to the null distribution. A significance level of 0.05 was chosen for comparison of modular partitions and global network properties.

Regional network properties were normalized by dividing by the mean of the corresponding regional network property across all regions before group comparisons (Bernhardt et al., 2011; Griffiths et al., 2016; Singh et al., 2013). Given the multiple analyses performed at the regional level, we corrected for multiple comparisons using a false-positive correction, $p < 1/(3 \times N)$, where N corresponds to the 74 GM regions. This procedure is equivalent to expecting less than one false positive across all tests per imaging contrast tested. We note that this procedure does not strongly control for type I error (Lynall et al., 2010). To provide further insight into this correction, we also calculated the proportion of permutations that yielded at least the same number of observed regional findings.

We next performed two sensitivity analyses. First, to more robustly remove global CBF and GMV effects from covariance matrices, we replaced our intensity-normalization step with the addition of global CBF or GMV as a covariate (alongside age, sex, BMI, race, and MRI site) prior to network construction. The second sensitivity analysis addressed the reliability of smaller regions in the atlas. To this end, we omitted 14 subcortical regions (bilateral amygdala, caudate, hippocampus, nucleus accumbens, putamen, thalamus, and uncus), thereby restricting our scope to the 60 cortical regions.

To assess the effect size of the observed differences between Lo- and Hi-WMH groups, we generated within-group distributions of all global and regional network properties with 10,000 bootstraps. Distributions of global and regional network properties were then used to calculate the standardized mean difference.

Post-hoc analyses investigated regional measures of CBF and GMV between Lo- and Hi-WMH groups in regions with significant findings. Independent samples t -tests were used at a significance level of 0.05. We also performed a direct element-by-element comparison of CBF and GMV covariance matrices between Lo- and Hi-WMH groups (see Supporting Information S1).

3 | RESULTS

3.1 | Demographic & clinical characteristics

The Lo- and Hi-WMH groups were matched for most demographic and clinical characteristics, presented in Table 1. Together, the mean age of the Lo- and Hi-WMH groups was 50 ± 3.6 years and 52% were female. Global CBF (Lo-WMH, 56.1 ± 12.3 ml/100 g/min; Hi-WMH, 56.6 ± 11.2 ml/100 g/min; $U = 7818.0$, $p = .34$) and GMV (Lo-WMH, 516.3 ± 55.3 ml; Hi-WMH, 521.5 ± 45.2 ml; $U = 7610.5$, $p = .44$) did

not differ between groups (Figure S1). There were, however, significant between-group differences in age (Lo-WMH, 50 ± 3.5 years of age; Hi-WMH, 51 ± 3.7 years of age; $U = 6708.5$, $p = .01$), sex (Lo-WMH, 40.0% female; Hi-WMH, 63.0% female; $\chi^2 = 12.36$, $p < .001$), BMI (Lo-WMH, 29.1 ± 5.0 kg/m²; Hi-WMH, 28.3 ± 5.3 kg/m²; $U = 7052.5$, $p = .04$), and high-density lipoprotein cholesterol (Lo-WMH, 56.4 ± 17.0 mg/dl; Hi-WMH, 60.7 ± 16.3 mg/dl; $U = 6649.5$, $p = .008$). As expected, WMH volume was significantly different between groups (Lo-WMH, 0.52 ± 0.22 ml; Hi-WMH, 2.87 ± 1.83 ml; $U = 0.0$, $p < .001$).

3.2 | Network modules

Consensus clustering derived three modules from CBF covariance networks that were not significantly different between Lo- and Hi-WMH groups (82.8% similar, $p = .559$) (Figure 2; Table S2). In the Lo-WMH group, Module 1 was the largest and encompassed inferior frontal, temporal, limbic, and subcortical brain regions. Module 2 was comprised of superior and medial frontal, parietal, and occipital brain regions. Module 3 included temporal, occipital, and limbic brain regions as well as the thalami. The Hi-WMH group modules were similar with exception of some discrepancies with the Lo-WMH group that were observed in occipital and temporal regions within Module 3.

From GMV covariance networks, we observed four and five modules from Lo- and Hi-WMH groups, that were not significantly different from each other (75.1% similar, $p = .395$). In the Lo-WMH group, Module 1 consisted of inferior frontal, limbic, parietal, and subcortical brain regions including the thalami. Module 2 consisted of occipital, temporal, and parietal brain regions. Module 3 included limbic, occipital, and temporal brain regions. Module 4 comprised temporal, superior and medial frontal, occipital, and parietal brain regions. In the Hi-WMH group, Module 1 retained subcortical, limbic, and parietal brain regions. Module 3 gained additional frontal and parietal brain regions. Finally, Module 5 consisted of limbic, inferior frontal, parietal, and temporal brain regions.

3.3 | Small-world properties

Across the range of network densities, both CBF and GMV covariance networks in both Lo- and Hi-WMH groups exhibited small-world properties, as quantified by a small-world coefficient greater than 1 (Figure 3). In other words, the ratio between the normalized clustering coefficient and the normalized characteristic path length was greater than 1 at all network densities.

3.4 | Global network properties

We found no significant between-group differences in clustering coefficient, characteristic path length, or global efficiency between CBF covariance networks (clustering coefficient, standardized mean difference = 0.04, $p = .97$; characteristic path length, standardized

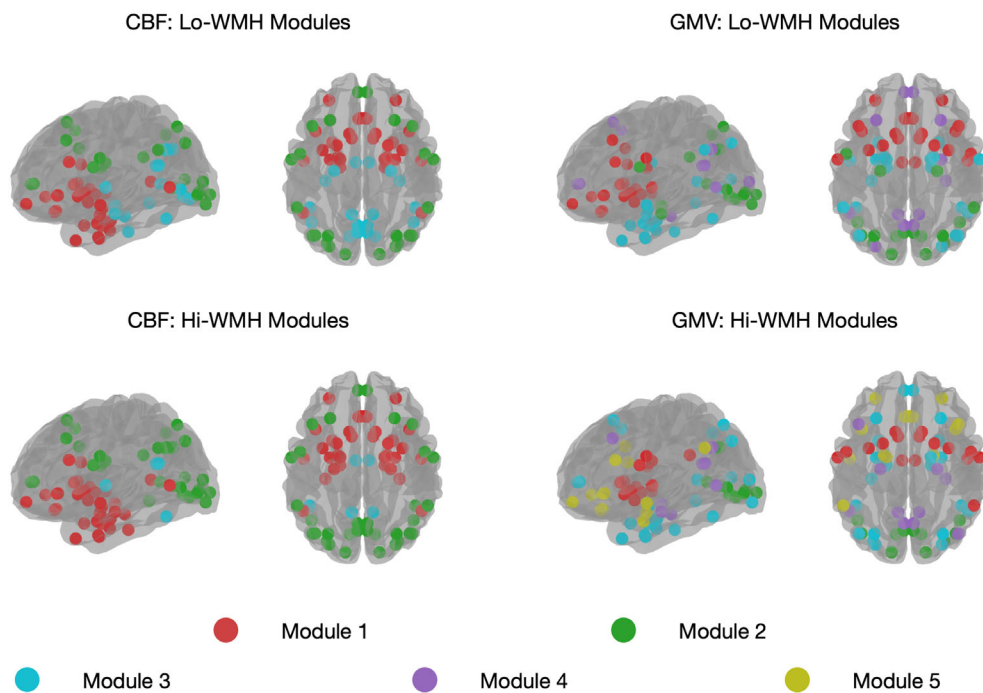


FIGURE 2 A depiction of the cerebral blood flow (CBF) and gray matter volume (GMV) covariance network modules are shown, as derived from consensus clustering. Parameter resolution values of 1.25 and 0.75 were chosen to generate modules from CBF and GMV covariance matrices using the Louvain community detection algorithm. Consensus clustering derived three modules from CBF covariance networks that were similar between Lo- and Hi-WMH groups. From GMV covariance networks, we observed four and five modules from Lo- and Hi-WMH groups respectively. WMH, white matter hyperintensities

Contrast	Region	Network property	Direction	<i>p</i>
CBF	R Putamen	Degree	Lo-WMH > Hi-WMH	.003
	L Nucleus Accumbens	Degree	Hi-WMH > Lo-WMH	.002
	L Nucleus Accumbens	Betweenness centrality	Hi-WMH > Lo-WMH	.002
GMV	L Lingual Gyrus	Degree	Lo-WMH > Hi-WMH	.003
	L Lingual Gyrus	Betweenness centrality	Lo-WMH > Hi-WMH	.004
	L Superior Occipital Gyrus	Local efficiency	Lo-WMH > Hi-WMH	.003
	R Superior Parietal Lobule	Local efficiency	Hi-WMH > Lo-WMH	.003

TABLE 2 Brain regions with significant group differences in regional network properties

Note: The threshold for statistical significance was set at $p < .0045$, in order to correct for multiple comparisons.

Abbreviations: CBF, cerebral blood flow; GMV, gray matter volume; L, left; R, right; WMH, white matter hyperintensity.

mean difference = 0.04, $p = .92$; global efficiency, standardized mean difference = 0.30, $p = .91$).

Similarly, there were no between-group differences between GMV covariance networks (clustering coefficient, standardized mean difference = 0.11, $p = .07$; characteristic path length, standardized mean difference = 0.17, $p = .30$; standardized mean difference = 0.17, global efficiency, $p = .29$) (Figure 4).

In our two sensitivity analyses (i.e., [1] regression of global CBF/GMV and [2] omission of subcortical regions), we similarly found no between-group differences in global network properties of CBF or GMV covariance networks (see Supporting Information S1).

3.5 | Regional network properties

Table 2 and Figure 5 present brain regions from CBF and GMV covariance networks with significant between-group differences in degree, betweenness centrality, and local efficiency. Within CBF covariance

networks, the Hi-WMH group had lower degree in the right putamen (standardized mean difference = 3.08, $p = .003$) relative to the Lo-WMH group. In contrast, the Hi-WMH group had higher degree (standardized mean difference = 3.85, $p = .002$) and betweenness centrality (standardized mean difference = 2.73, $p = .002$) in the left nucleus accumbens. We observed no between-group differences in local efficiency within CBF covariance networks.

Within GMV covariance networks, the Hi-WMH group had lower degree (standardized mean difference = 1.83, $p = .003$) and betweenness centrality (standardized mean difference = 1.60, $p = .004$) in the left lingual gyrus and lower local efficiency (standardized mean difference = 0.76, $p = .003$) in the left superior occipital gyrus. In contrast, the Hi-WMH group had higher local efficiency (standardized mean difference = 1.69, $p = .003$) in the right superior parietal lobule.

Of the 10,000 permutations performed, we found that 297 of them resulted in at least seven regional findings at a significance level of $p < 1/(3 \times N)$. Post-hoc analyses investigating regional measures of CBF and GMV in the above regions of interest revealed no significant

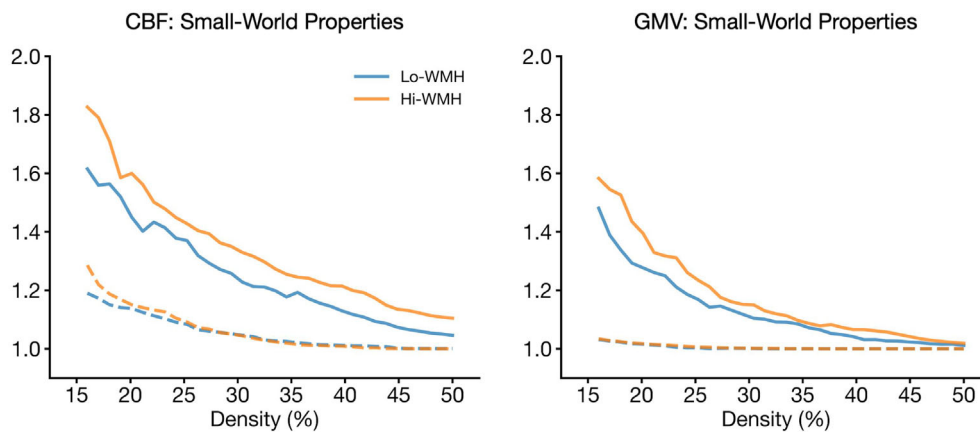


FIGURE 3 Small-world properties of cerebral blood flow (left) and gray matter volume (right) covariance matrices as a function of network density for Lo- (blue) and Hi-WMH (orange) groups. The small-world coefficient is defined as the ratio between normalized clustering coefficient (solid lines) and normalized characteristic path length (dashed lines). Both Lo- and Hi-WMH groups exhibited small-world topologies (i.e., the ratio between normalized clustering coefficient and normalized characteristic path length is greater than 1). Networks were normalized by 100 random networks that preserved the number of nodes and edges as well as the degree of individual nodes. Note that the y-axis is normalized and unitless. WMH, white matter hyperintensities

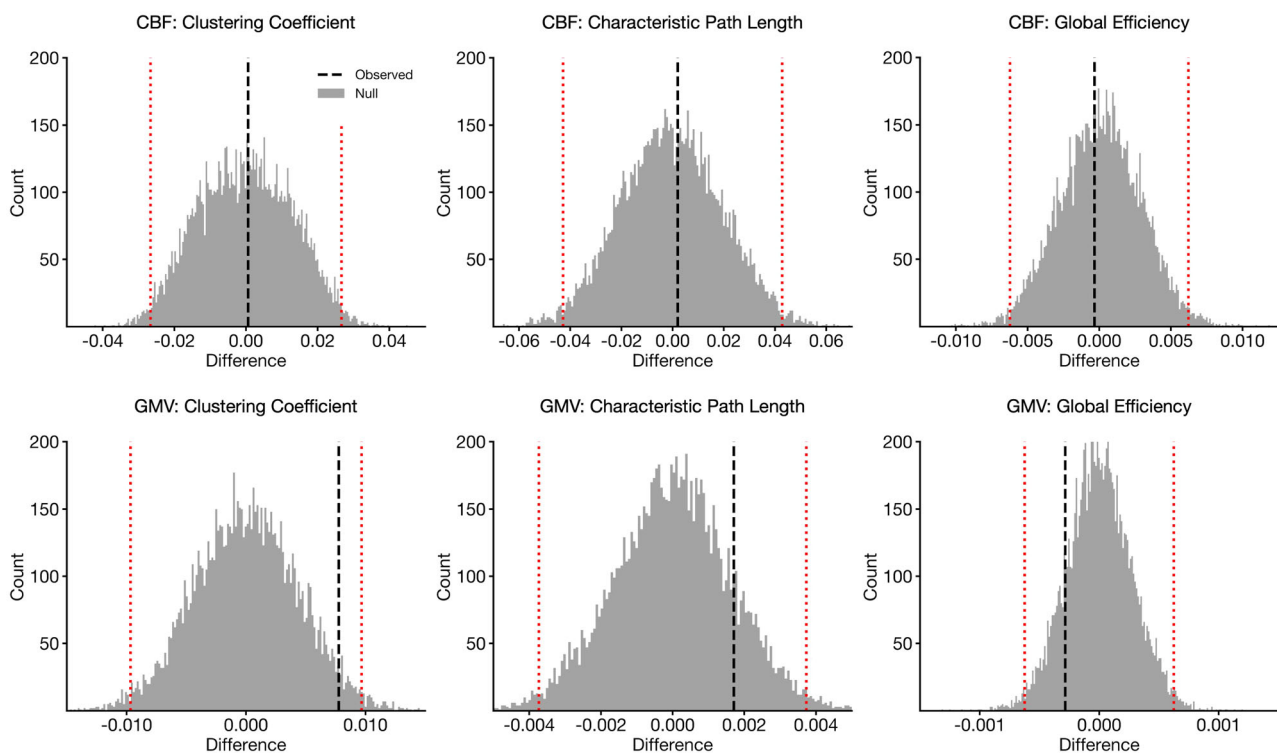


FIGURE 4 Differences in global network properties in cerebral blood flow (CBF) (top row) and gray matter volume (GMV) (bottom row) covariance networks. Vertical dashed lines indicate observed differences between Lo- and Hi-WMH groups (Hi-WMH – Lo-WMH). Histograms illustrate null distributions and red dotted lines indicate 95% confidence intervals as derived from the nonparametric permutation procedure. There were no significant between-group differences in any of the global network properties for either CBF or GMV covariance networks at $p < .05$. WMH, white matter hyperintensities

between-group differences (Table 3). Finally, a direct element-by-element comparison of CBF and GMV covariance matrices revealed no significant between-group differences (see Supporting Information S1).

The findings from our two sensitivity analyses (i.e., [1] regression of global CBF/GMV and [2] omission of subcortical regions) were consistent with these results (see Supporting Information S1).

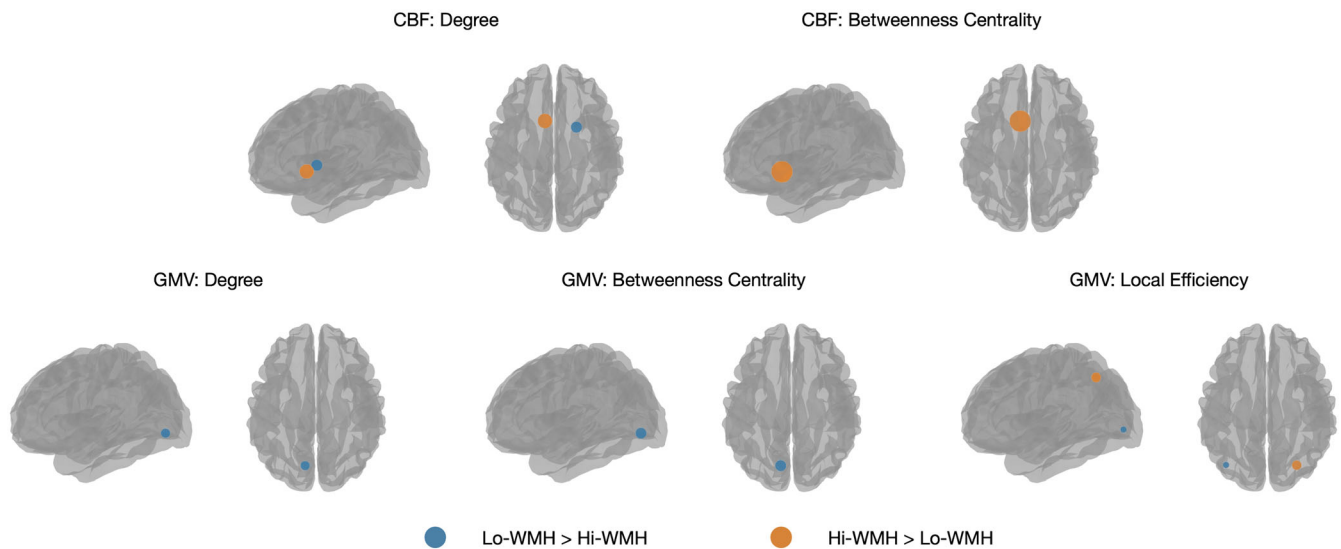


FIGURE 5 Brain regions that exhibited significant between-group differences in regional network properties are shown as blue or orange spheres. Blue corresponds to Lo-WMH > Hi-WMH, while orange corresponds to Hi-WMH > Lo-WMH. Sphere size corresponds to the magnitude of the group difference. The threshold for statistical significance was set at $p < .0045$, in order to correct for multiple comparisons. WMH, white matter hyperintensities

TABLE 3 Post-hoc analyses investigating absolute measures of CBF and GMV in regions-of-interest

Contrast	Region	Lo-WMH	Hi-WMH	Test statistic	<i>p</i>
CBF (ml/100 g/min)	R Putamen	48.04 ± 10.27	47.42 ± 10.34	$t = 0.48$.63
	L Nucleus Accumbens	51.08 ± 13.31	50.82 ± 14.21	$t = 0.15$.88
GMV (ml)	L Lingual Gyrus	4.05 ± 0.94	4.18 ± 0.88	$t = 1.15$.25
	L Superior Occipital Gyrus	4.94 ± 1.07	4.91 ± 1.03	$t = 0.25$.81
	R Superior Parietal Lobule	15.09 ± 2.30	14.94 ± 2.21	$t = 0.53$.60

Note: Independent samples *t*-tests were used to compare regional measures of CBF and GMV between Lo- and Hi-WMH groups. No significant differences were observed at a threshold of $p < .05$.

Abbreviations: CBF, cerebral blood flow; GMV, gray matter volume; L, left; R, right; WMH, white matter hyperintensity.

4 | DISCUSSION

In this study, we used graph theory to compare CBF and GMV covariance networks among midlife adults with lower and higher levels of WMH volume. First, we performed a community detection analysis on CBF and GMV covariance networks, resulting in modules of brain regions that were largely consistent between groups. Next, we found that both CBF and GMV covariance networks exhibited small-world topologies across a range of network densities. Finally, we compared CBF and GMV covariance network topologies between groups and found that higher WMH volume was not accompanied by alterations to global network properties. In contrast, higher WMH volume was related to altered degree, betweenness centrality, and local efficiency in several brain regions within both CBF and GMV covariance networks. Altogether, these findings provide a picture of physiological and structural patterns across the brain and point to WMH-related network changes in midlife adults.

We first performed community detection analyses to detect modules of brain regions that tend to covary with each other in CBF and

GMV covariance networks. CBF covariance matrices were partitioned into three modules that were consistent between Lo- and Hi-WMH groups. Using ASL, Luciw et al. found that communities derived from CBF covariance patterns in adolescents are spatially similar to the brain's vascular territories (Luciw et al., 2021). Using single-photon emission computed tomography (SPECT), Melie-García et al. observed that the strongest CBF covariance patterns occurred between bilateral brain regions in healthy adults (Melie-García et al., 2013). The present study's findings are similar in both respects, with CBF covariance modules encompassing bilateral brain regions and partially demarcating the brain's vascular territories. Meanwhile, GMV covariance matrices were partitioned into four and five modules from Lo- and Hi-WMH groups, respectively. While modules were not significantly different between groups, there were subtle differences between partitions. For instance, Module 1 (frontal and subcortical) in the Lo-WMH group was divided into Modules 1 (subcortical) and 5 (frontal) in the Hi-WMH group. These changes to modular organization could therefore be reflective of early alterations to normal covariance patterns as a consequence of higher WMH volume in midlife.

Next, we found that both CBF and GMV covariance networks exhibited small-world topologies, indicating a balance between functional segregation and functional integration (Watts & Strogatz, 1998). Small-world networks are thought to be effectively configured so as to combine clusters of specialized nodes with strategically positioned intermediary edges that minimize overall path lengths, thus improving communication efficiency. These nonrandom properties have been recapitulated across a wide range of neuroimaging techniques, providing evidence that the brain exhibits a complex yet efficient topology to augment information processing (Bullmore & Sporns, 2009). The current study's findings support this hypothesis by demonstrating that networks derived from CBF and GMV covariance analysis similarly obey this organizational structure.

In comparing Lo- and Hi-WMH groups, we observed no global between-group differences in the clustering coefficient, characteristic path length, or global efficiency of either CBF or GMV covariance networks. These findings imply that in this sample of midlife adults, the functional integration and segregation of CBF and GMV covariance networks were not affected by higher WMH volume. It is worth noting that in the CARDIA study, WMH volume may be sufficiently high to alter physiological and structural aspects of brain health, but is still low compared to other prospective studies of SVD (Nasrallah, Hsieh, et al., 2019). For instance, other studies reporting on older individuals with comparatively higher WMH volume have found more widespread disruption of structural covariance networks to be associated with higher WMH volume (Nestor et al., 2017). Another factor may be the presence of compensatory mechanisms that resist global network changes brought upon by higher WMH volume. For instance, others have posited that regions of increased CBF may counteract WMH-related deficiencies elsewhere, which may therefore suppress CBF covariance changes (Stewart et al., 2021). Altogether, while no global between-group differences were observed in this cross-sectional study, it may be an accumulation of SVD lesions beginning in midlife that leads to progressively worsening network deficits (Tuladhar et al., 2015).

While the absence of between-group differences in global network properties is at least partially attributable to the relatively low WMH volume seen in this sample of midlife adults, it may also be a consequence of the choice of imaging modalities and subsequent network analyses performed in this study. Indeed, studies of SVD through the lens of more traditional network imaging modalities, such as DTI or fMRI, have observed diverging results. For instance, Lawrence et al. found that in an older sample of individuals with severe SVD (mean age = 65.9 ± 11.7 years, mean WMH volume = 33 ± 34 ml), DTI-based analyses of structural connectivity demonstrated widespread topological deficits, while fMRI-based analyses in the same sample resulted in no such changes (Lawrence et al., 2018). Meanwhile, Frey et al. observed DTI-based global network disturbances even in adults with mild SVD (median age = 64 years, median WMH volume = 0.6 ml) (Frey et al., 2020). It is important, therefore, to highlight methodological effects on results arising from such network analytic studies; although no global between-group differences were observed here through CBF and GMV covariance, it may be that

DTI- or fMRI-based analyses observe divergent findings. Future work is needed to study CBF and GMV covariance in relation to DTI or fMRI, with an emphasis on SVD.

In contrast, we report significant regional between-group differences in the degree, betweenness centrality, and local efficiency of several distributed brain regions within both CBF and GMV covariance networks. Namely, we observed CBF covariance alterations in brain regions of the basal ganglia (putamen, nucleus accumbens) while GMV covariance revealed alterations in brain regions of the visual (lingual gyri, superior occipital gyrus) and dorsal attention (superior parietal lobule) networks. The chosen regional network properties are reflective of the importance and influence of individual nodes within a network; in the context of CBF and GMV covariance, these network properties describe the nature of and extent to which individual brain regions connect (i.e., covary) with others as well as the impact of these connections on the overall network. The regional and widespread nature of these network alterations, therefore, could reflect subtle WMH-related physiological and structural changes beginning in early stages of disease, and may precede larger network-wide breakdown as reported in more severe stages of SVD (Frey et al., 2020; Lawrence et al., 2014; Petersen et al., 2020; Reginold et al., 2019; Tuladhar et al., 2016; Xu et al., 2018). Similarly, deficits in regional brain physiology and structure are known to be associated with SVD severity as indexed by increasing WMH volume (Crane et al., 2015; Habes et al., 2016; C. M. Kim et al., 2020; Tuladhar et al., 2015; Tullberg et al., 2004). Multivariate covariance may therefore supplement such univariate analyses in detecting earlier or distinct disease-related alterations and in pursuing novel biomarker or hypothesis-generating findings (Wee et al., 2013). Notably, our post-hoc analyses examining absolute measures of CBF and GMV in brain regions with significant topological differences revealed no significant between-group differences.

This study has several limitations. First, by virtue of our study design, we sought to establish group-level covariance networks, which limits our ability to comment on individual participants. While individualized covariance networks are feasible, it has been shown that individual variability in regional measures may impact subsequent graph theory analyses (H. J. Kim et al., 2016). Second, our group stratification procedure resulted in a decreased sample size. While our analyses retained only a proportion of the original cohort, this procedure resulted in two groups clearly delineated by WMH burden. Third, our false-positive correction does not strongly correct for Type I error. Given the number of regional comparisons made, we chose to avoid an overly conservative correction at the risk of an increased number of false positives. Therefore, although this study benefitted from a large sample size and a permutation-based analysis, caution is warranted in interpreting the regional findings. Fourth, the choice of parcellation scheme has been shown to affect brain network estimates (Messé, 2020). It is, however, important to note that this choice has been evaluated mainly in the context of more traditional forms of brain network analysis (i.e., functional connectivity via fMRI, structural connectivity via DTI), and not covariance analysis (Arslan et al., 2018; Zalesky et al., 2010). Indeed, other covariance studies that do report

on several atlases show little to no effect on downstream results (Alexander-Bloch, Raznahan, et al., 2013; Liu et al., 2016; Luciw et al., 2021). Validation studies using external cohort data and alternative parcellation schemes would be desirable to corroborate the findings of the current study. Fifth, the ASL data was acquired at a low spatial resolution and may therefore be susceptible to partial volume effects, particularly in smaller brain regions. While correction for such effects is desirable, such procedures often rely on many subsidiary steps in the processing pipeline (i.e., registration, segmentation, data smoothing, accuracy of WMH segmentation) that are difficult to accurately implement. Finally, the current study was agnostic to WMH location, instead choosing to study generalizable WMH-related effects on covariance networks. Furthermore, while our focus was limited to WMHs, it is important to note that other markers of SVD (e.g., lacunar infarcts, enlarged perivascular spaces) were not accounted for in this study. Therefore, future work is needed to consider the effects of other markers of SVD on covariance networks and how lesion location may mediate this relationship.

In conclusion, we used CBF and GMV covariance analysis to detect WMH-related network changes in midlife adults. We observed modular organization in both CBF and GMV covariance networks that was consistent between Lo- and Hi-WMH groups. We furthermore found that both CBF and GMV covariance networks exhibited small-world properties in both Lo- and Hi-WMH groups, implying an effective balance between functional integration and segregation. We observed no significant between-group differences when considering global network properties, suggesting no detectable expression of widespread WMH-related disruptions to functional integration and segregation in this sample of midlife adults. We did, however, detect alterations to regional network properties of CBF and GMV covariance networks in the Hi-WMH group, which may imply the start of a separation that progresses with age and SVD severity. These findings identify potential WMH-related network alterations in midlife and provide possible avenues for further research of structural and functional brain changes in SVD.

ACKNOWLEDGMENTS

The CARDIA study is conducted and supported by the National Heart, Lung, and Blood Institute (NHLBI) in collaboration with the University of Alabama at Birmingham (HHSN268201800005I & HHSN268201800007I), Northwestern University (HHSN268201800003I), University of Minnesota (HHSN268201800006I), and Kaiser Foundation Research Institute (HHSN268201800004I). CARDIA was also partially supported by the Intramural Research Program of the National Institute on Aging (NIA) and an intra-agency agreement between NIA and NHLBI (AG0005). This manuscript has been reviewed by CARDIA for scientific content. William S. H. Kim received funding from a CIHR CGS-M award. Bradley J. MacIntosh received funding from a NARSAD Independent Investigator Grant from the Brain and Behaviour Research Foundation and a CIHR Project Grant (165981). Bradley J. MacIntosh also acknowledges the Dr. Sandra Black Centre for Brain Resilience & Recovery.

CONFLICT OF INTEREST

The authors declare no competing interests.

DATA AVAILABILITY STATEMENT

Data in this study are from a subset of men and women who participated in the community-based Coronary Artery Risk Development in Young Adults (CARDIA) brain MRI substudy, examined at the 25-year follow-up exam. Data access is available through the CARDIA Coordinating Center following approval by the CARDIA Publications and Presentations Committee.

ORCID

William S. H. Kim  <https://orcid.org/0000-0003-1257-1348>
 Nicholas J. Luciw  <https://orcid.org/0000-0003-4043-990X>
 Sarah Atwi  <https://orcid.org/0000-0003-2312-2281>
 Zahra Shirzadi  <https://orcid.org/0000-0001-6854-9356>
 Sudipto Dolui  <https://orcid.org/0000-0002-9035-3795>
 John A. Detre  <https://orcid.org/0000-0002-8115-6343>
 Ilya M. Nasrallah  <https://orcid.org/0000-0003-2346-7562>
 Walter Swardfager  <https://orcid.org/0000-0002-0030-8908>
 Robert Nick Bryan  <https://orcid.org/0000-0002-2327-4579>
 Lenore J. Launer  <https://orcid.org/0000-0002-3238-7612>
 Bradley J. MacIntosh  <https://orcid.org/0000-0001-7300-2355>

REFERENCES

- Alexander-Bloch, A., Giedd, J. N., & Bullmore, E. (2013). Imaging structural co-variance between human brain regions. *Nature Reviews Neuroscience*, 14, 322–336. <https://doi.org/10.1038/nrn3465>
- Alexander-Bloch, A., Raznahan, A., Bullmore, E., & Giedd, J. (2013). The convergence of maturational change and structural covariance in human cortical networks. *Journal of Neuroscience*, 33, 2889–2899. <https://doi.org/10.1523/JNEUROSCI.3554-12.2013>
- American Diabetes Association. (2011). Diagnosis and classification of diabetes mellitus. *Diabetes Care*, 34, S62–S69. <https://doi.org/10.2337/dc11-S062>
- Appelman, A. P. A., Exalto, L. G., Van Der Graaf, Y., Biessels, G. J., Mali, W. P. T. M., & Geerlings, M. I. (2009). White matter lesions and brain atrophy: More than shared risk factors? A systematic review. *Cerebrovascular Diseases*, 28, 227–242. <https://doi.org/10.1159/000226774>
- Arslan, S., Ktena, S. I., Makropoulos, A., Robinson, E. C., Rueckert, D., & Parisot, S. (2018). Human brain mapping: A systematic comparison of parcellation methods for the human cerebral cortex. In *NeuroImage* (Vol. 170, pp. 5–30). Neuroimage. <https://doi.org/10.1016/j.neuroimage.2017.04.014>
- Baezner, H., Blahak, C., Poggesi, A., Pantoni, L., Inzitari, D., Chabriat, H., Erkinjuntti, T., Fazekas, F., Ferro, J. M., Langhorne, P., O'Brien, J., Scheltens, P., Visser, M. C., Wahlund, L. O., Waldemar, G., Wallin, A., & Hennerici, M. G. (2008). Association of gait and balance disorders with age-related white matter changes: The LADIS study. *Neurology*, 70, 935–942. <https://doi.org/10.1212/01.wnl.0000305959.46197.e6>
- Bernhardt, B. C., Chen, Z., He, Y., Evans, A. C., & Bernasconi, N. (2011). Graph-theoretical analysis reveals disrupted small-world organization of cortical thickness correlation networks in temporal lobe epilepsy. *Cerebral Cortex*, 21(9), 2147–2157. <https://doi.org/10.1093/cercor/bhq291>
- Blondel, V. D., Guillaume, J. L., Lambiotte, R., & Lefebvre, E. (2008). Fast unfolding of communities in large networks. *Journal of Statistical*

- Mechanics: Theory and Experiment*, 2008(10), 10008. <https://doi.org/10.1088/1742-5468/2008/10/P10008>
- Bryan, R. N., Cai, J., Burke, G., Hutchinson, R. G., Liao, D., Toole, J. F., Dagher, A. P., & Cooper, L. (1999). Prevalence and anatomic characteristics of infarct-like lesions on MR images of middle-aged adults: The atherosclerosis risk in communities study. *American Journal of Neurology*, 20, 1273–1280.
- Bullmore, E., & Sporns, O. (2009). Complex brain networks: Graph theoretical analysis of structural and functional systems. *Nature Reviews Neuroscience*, 10, 186–198. <https://doi.org/10.1038/nrn2575>
- Cannistraro, R. J., Badi, M., Eidelman, B. H., Dickson, D. W., Middlebrooks, E. H., & Meschia, J. F. (2019). CNS small vessel disease: A clinical review. *Neurology*, 92, 1146–1156. <https://doi.org/10.1212/WNL.0000000000007654>
- Chen, H., Huang, L., Yang, D., Ye, Q., Guo, M., Qin, R., Luo, C., Li, M., Ye, L., Zhang, B., & Xu, Y. (2019). Nodal global efficiency in front-parietal lobe mediated periventricular white matter hyperintensity (PWMH)-related cognitive impairment. *Frontiers in Aging Neuroscience*, 11, 347. <https://doi.org/10.3389/fnagi.2019.00347>
- Cohen, J. R., & D'Esposito, M. (2016). The segregation and integration of distinct brain networks and their relationship to cognition. *Journal of Neuroscience*, 36(48), 12083–12094. <https://doi.org/10.1523/JNEUROSCI.2965-15.2016>
- Crane, D. E., Black, S. E., Ganda, A., Mikulis, D. J., Nestor, S. M., Donahue, M. J., & MacIntosh, B. J. (2015). Grey matter blood flow and volume are reduced in association with white matter hyperintensity lesion burden: A cross-sectional MRI study. *Frontiers in Aging Neuroscience*, 7, 131. <https://doi.org/10.3389/fnagi.2015.00131>
- d'Arbeloff, T., Elliott, M. L., Knodt, A. R., Melzer, T. R., Keenan, R., Ireland, D., Ramrakha, S., Poulton, R., Anderson, T., Caspi, A., Moffitt, T. E., & Hariri, A. R. (2019). White matter hyperintensities are common in mid-life and already associated with cognitive decline. *Brain Communications*, 1, fcz041. <https://doi.org/10.1093/braincomms/fcz041>
- De Groot, J. C., De Leeuw, F. E., Oudkerk, M., Hofman, A., Jolles, J., & Breteler, M. M. B. (2001). Cerebral white matter lesions and subjective cognitive dysfunction: The Rotterdam scan study. *Neurology*, 56, 1539–1545. <https://doi.org/10.1212/WNL.56.11.1539>
- De Laat, K. F., Tuladhar, A. M., Van Norden, A. G. W., Norris, D. G., Zwiers, M. P., & De Leeuw, F. E. (2011). Loss of white matter integrity is associated with gait disorders in cerebral small vessel disease. *Brain*, 134, 73–83. <https://doi.org/10.1093/brain/awq343>
- De Leeuw, F. E., De Groot, J. C., Oudkerk, M., Wittteman, J. C. M., Hofman, A., Van Gijn, J., & Breteler, M. M. B. (1999). A follow-up study of blood pressure and cerebral white matter lesions. *Annals of Neurology*, 46(6), 827.
- Di, X., Gohel, S., Thielcke, A., Wehrl, H. F., & Biswal, B. B. (2017). Do all roads lead to Rome? A comparison of brain networks derived from inter-subject volumetric and metabolic covariance and moment-to-moment hemodynamic correlations in old individuals. *Brain Structure and Function*, 222(8), 3833–3845. <https://doi.org/10.1007/s00429-017-1438-7>
- Dolui, S., Wang, Z., Wang, D. J. J., Mattay, R., Finkel, M., Elliott, M., Desiderio, L., Inglis, B., Mueller, B., Stafford, R. B., Launer, L. J., Jacobs, D. R., Bryan, R. N., & Detre, J. A. (2016). Comparison of non-invasive MRI measurements of cerebral blood flow in a large multisite cohort. *Journal of Cerebral Blood Flow and Metabolism*, 36, 1244–1256. <https://doi.org/10.1177/0271678X16646124>
- Frey, B. M., Petersen, M., Schlemm, E., Mayer, C., Hanning, U., Engelke, K., Fiehler, J., Borof, K., Jagodzinski, A., Gerloff, C., Thomalla, G., & Cheng, B. (2020). White matter integrity and structural brain network topology in cerebral small vessel disease: The Hamburg city health study. *Human Brain Mapping*, 42(5), 1406–1415. <https://doi.org/10.1002/hbm.25301>
- Godin, O., Maillard, P., Crivello, F., Alperovitch, A., Mazoyer, B., Tzourio, C., & Dufouil, C. (2009). Association of white-matter lesions with brain atrophy markers: The three-city Dijon MRI study. *Cerebrovascular Diseases*, 28, 177–184. <https://doi.org/10.1159/000226117>
- Goldszal, A. F., Davatzikos, C., Pham, D. L., Yan, M. X. H., Bryan, R. N., & Resnick, S. M. (1998). An image-processing system for qualitative and quantitative volumetric analysis of brain images. *Journal of Computer Assisted Tomography*, 22, 827–837. <https://doi.org/10.1097/00004728-199809000-00030>
- Gong, G., He, Y., Chen, Z. J., & Evans, A. C. (2012). Convergence and divergence of thickness correlations with diffusion connections across the human cerebral cortex. *NeuroImage*, 59, 1239–1248. <https://doi.org/10.1016/j.neuroimage.2011.08.017>
- Griffiths, K. R., Grieve, S. M., Kohn, M. R., Clarke, S., Williams, L. M., & Korgaonkar, M. S. (2016). Altered gray matter organization in children and adolescents with ADHD: A structural covariance connectome study. *Translational Psychiatry*, 6, e947. <https://doi.org/10.1038/tp.2016.219>
- Habes, M., Erus, G., Toledo, J. B., Zhang, T., Bryan, N., Launer, L. J., Rosseel, Y., Janowitz, D., Doshi, J., Van Der Auwera, S., Von Sarnowski, B., Hegenscheid, K., Hosten, N., Homuth, G., Völzke, H., Schminke, U., Hoffmann, W., Grabe, H. J., & Davatzikos, C. (2016). White matter hyperintensities and imaging patterns of brain ageing in the general population. *Brain*, 139(4), 1164–1179. <https://doi.org/10.1093/brain/aww008>
- Kabani, N. J., Collins, D. L., & Evans, A. C. (1998). A 3D neuroanatomical atlas. *Fourth International Conference on Functional Mapping of the Human Brain*, 7, 12.
- Kelly, C., Toro, R., Di Martino, A., Cox, C. L., Bellec, P., Castellanos, F. X., & Milham, M. P. (2012). A convergent functional architecture of the insula emerges across imaging modalities. *NeuroImage*, 61, 1129–1142. <https://doi.org/10.1016/j.neuroimage.2012.03.021>
- Kim, C. M., Alvarado, R. L., Stephens, K., Wey, H. Y., Wang, D. J. J., Leritz, E. C., & Salat, D. H. (2020). Associations between cerebral blood flow and structural and functional brain imaging measures in individuals with neuropsychologically defined mild cognitive impairment. *Neurobiology of Aging*, 86, 64–74. <https://doi.org/10.1016/j.neurobiolaging.2019.10.023>
- Kim, H. J., Shin, J. H., Han, C. E., Kim, H. J., Na, D. L., Seo, S. W., & Seong, J. K. (2016). Using individualized brain network for analyzing structural covariance of the cerebral cortex in Alzheimer's patients. *Frontiers in Neuroscience*, 10, 394. <https://doi.org/10.3389/fnins.2016.00394>
- Lancichinetti, A., & Fortunato, S. (2012). Consensus clustering in complex networks. *Scientific Reports*, 2(1), 1–7. <https://doi.org/10.1038/srep00336>
- Launer, L. J., Lewis, C. E., Schreiner, P. J., Sidney, S., Battapady, H., Jacobs, D. R., Lim, K. O., D'Esposito, M., Zhang, Q., Reis, J., Davatzikos, C., & Bryan, R. N. (2015). Vascular factors and multiple measures of early brain health: CARDIA brain MRI study. *PLoS ONE*, 10, e0122138. <https://doi.org/10.1371/journal.pone.0122138>
- Lawrence, A. J., Chung, A. W., Morris, R. G., Markus, H. S., & Barrick, T. R. (2014). Structural network efficiency is associated with cognitive impairment in small-vessel disease. *Neurology*, 83, 304–311. <https://doi.org/10.1212/WNL.0000000000000612>
- Lawrence, A. J., Tozer, D. J., Stamatakis, E. A., & Markus, H. S. (2018). A comparison of functional and tractography based networks in cerebral small vessel disease. *NeuroImage: Clinical*, 18, 425–432. <https://doi.org/10.1016/j.nicl.2018.02.013>
- Liu, F., Zhuo, C., & Yu, C. (2016). Altered cerebral blood flow covariance network in schizophrenia. *Frontiers in Neuroscience*, 10, 308. <https://doi.org/10.3389/fnins.2016.00308>
- Luciw, N. J., Toma, S., Goldstein, B. I., & MacIntosh, B. J. (2021). Correspondence between patterns of cerebral blood flow and structure in adolescents with and without bipolar disorder. *Journal of Cerebral Blood Flow & Metabolism*, 41, 1988–1999. <https://doi.org/10.1177/0271678X21989246>

- Lynall, M. E., Bassett, D. S., Kerwin, R., McKenna, P. J., Kitzbichler, M., Muller, U., & Bullmore, E. (2010). Functional connectivity and brain networks in schizophrenia. *Journal of Neuroscience*, 30, 9477–9487. <https://doi.org/10.1523/JNEUROSCI.0333-10.2010>
- Mahinrad, S., Kurian, S., Garner, C. R., Sedaghat, S., Nemeth, A. J., Moscufo, N., Higgins, J. P., Jacobs, D. R., Hausdorff, J. M., Lloyd-Jones, D. M., & Sorond, F. A. (2020). Cumulative blood pressure exposure during young adulthood and mobility and cognitive function in midlife. *Circulation*, 141(9), 712–724. <https://doi.org/10.1161/CIRCULATIONAHA.119.042502>
- Medley, M. L. (1980). Life satisfaction across four stages of adult life. *International Journal of Aging and Human Development*, 11(3), 193–209.
- Melie-García, L., Sanabria-Díaz, G., & Sánchez-Catasús, C. (2013). Studying the topological organization of the cerebral blood flow fluctuations in resting state. *NeuroImage*, 64, 173–184. <https://doi.org/10.1016/j.neuroimage.2012.08.082>
- Messé, A. (2020). Parcellation influence on the connectivity-based structure–function relationship in the human brain. *Human Brain Mapping*, 41, 1167–1180. <https://doi.org/10.1002/hbm.24866>
- Nasrallah, I. M., Hsieh, M. K., Erus, G., Battapady, H., Dolui, S., Detre, J. A., Launer, L. J., Jacobs, D. R., Davatzikos, C., & Bryan, R. N. (2019). White matter lesion penumbra shows abnormalities on structural and physiologic MRIs in the coronary artery risk development in young adults cohort. *American Journal of Neuroradiology*, 40, 1291–1298. <https://doi.org/10.3174/ajnr.A6119>
- Nasrallah, I. M., Pajewski, N. M., Auchus, A. P., Chelune, G., Cheung, A. K., Cleveland, M. L., Coker, L. H., Crowe, M. G., Cushman, W. C., Cutler, J. A., Davatzikos, C., Desiderio, L., Doshi, J., Erus, G., Fine, L. J., Gaussoin, S. A., Harris, D., Johnson, K. C., Kimmel, P. L., ... Bryan, R. N. (2019). Association of intensive vs standard blood pressure control with cerebral white matter lesions. *JAMA*, 322, 524–534. <https://doi.org/10.1001/jama.2019.10551>
- Nestor, S. M., Mišić, B., Ramirez, J., Zhao, J., Graham, S. J., Verhoeff, N. P. L. G., Stuss, D. T., Masellis, M., & Black, S. E. (2017). Small vessel disease is linked to disrupted structural network covariance in Alzheimer's disease. *Alzheimer's and Dementia*, 13, 749–760. <https://doi.org/10.1016/j.jalz.2016.12.007>
- Petersen, M., Frey, B. M., Schlemm, E., Mayer, C., Hanning, U., Engelke, K., Fiehler, J., Borof, K., Jagodzinski, A., Gerloff, C., Thomalla, G., & Cheng, B. (2020). Network localisation of white matter damage in cerebral small vessel disease. *Scientific Reports*, 10(1), 9210. <https://doi.org/10.1038/s41598-020-66013-w>
- Rabins, P. V., Pearlson, G. D., Aylward, E., Kumar, A. J., & Dowell, K. (1991). Cortical magnetic resonance imaging changes in elderly inpatients with major depression. *American Journal of Psychiatry*, 148, 617–620. <https://doi.org/10.1176/ajp.148.5.617>
- Reginold, W., Sam, K., Poublanc, J., Fisher, J., Crawley, A., & Mikulis, D. J. (2019). The efficiency of the brain connectome is associated with cerebrovascular reactivity in persons with white matter hyperintensities. *Human Brain Mapping*, 40(12), 3647–3656. <https://doi.org/10.1002/hbm.24622>
- Reijmer, Y. D., Fotiadis, P., Piantoni, G., Boulouis, G., Kelly, K. E., Guro, M. E., Leemans, A., O'Sullivan, M. J., Greenberg, S. M., & Viswanathan, A. (2016). Small vessel disease and cognitive impairment: The relevance of central network connections. *Human Brain Mapping*, 37, 2446–2454. <https://doi.org/10.1002/hbm.23186>
- Rossi, R., Boccardi, M., Sabatoli, F., Galluzzi, S., Alaimo, G., Testa, C., & Frisoni, G. B. (2006). Topographic correspondence between white matter hyperintensities and brain atrophy. *Journal of Neurology*, 253, 919–927. <https://doi.org/10.1007/s00415-006-0133-z>
- Rubinov, M., & Sporns, O. (2010). Complex network measures of brain connectivity: Uses and interpretations. *NeuroImage*, 52, 1059–1069. <https://doi.org/10.1016/j.neuroimage.2009.10.003>
- Sang, L., Chen, L., Wang, L., Zhang, J., Zhang, Y., Li, P., Li, C., & Qiu, M. (2018). Progressively disrupted brain functional connectivity network in subcortical ischemic vascular cognitive impairment patients. *Frontiers in Neurology*, 9, 94. <https://doi.org/10.3389/fneur.2018.00094>
- Schaefer, A., Quinque, E. M., Kipping, J. A., Arélin, K., Roggenhofer, E., Frisch, S., Villringer, A., Mueller, K., & Schroeter, M. L. (2014). Early small vessel disease affects frontoparietal and cerebellar hubs in close correlation with clinical symptoms – a resting-state fMRI study. *Journal of Cerebral Blood Flow and Metabolism*, 34, 1091–1095. <https://doi.org/10.1038/jcbfm.2014.70>
- Schmidt, R., Ropele, S., Enzinger, C., Petrovic, K., Smith, S., Schmidt, H., Matthews, P. M., & Fazekas, F. (2005). White matter lesion progression, brain atrophy, and cognitive decline: The Austrian stroke prevention study. *Annals of Neurology*, 58, 610–616. <https://doi.org/10.1002/ana.20630>
- Shen, D., & Davatzikos, C. (2002). HAMMER: Hierarchical attribute matching mechanism for elastic registration. *IEEE Transactions on Medical Imaging*, 21(11), 1421–1439. <https://doi.org/10.1109/TMI.2002.803111>
- Singh, M. K., Kesler, S. R., Hadi Hosseini, S. M., Kelley, R. G., Amatya, D., Hamilton, J. P., Chen, M. C., & Gotlib, I. H. (2013). Anomalous gray matter structural networks in major depressive disorder. *Biological Psychiatry*, 74(10), 777–785. <https://doi.org/10.1016/j.biopsych.2013.03.005>
- Smith, E. E., O'Donnell, M., Dagenais, G., Lear, S. A., Wielgosz, A., Sharma, M., Poirier, P., Stotts, G., Black, S. E., Strother, S., Noseworthy, M. D., Benavente, O., Modi, J., Goyal, M., Batool, S., Sanchez, K., Hill, V., McCreary, C. R., Frayne, R., ... Yusuf, S. (2015). Early cerebral small vessel disease and brain volume, cognition, and gait. *Annals of Neurology*, 77, 251–261. <https://doi.org/10.1002/ana.24320>
- Stewart, C. R., Stringer, M. S., Shi, Y., Thrippleton, M. J., & Wardlaw, J. M. (2021). Associations between white matter hyperintensity burden, cerebral blood flow and transit time in small vessel disease: An updated meta-analysis. *Frontiers in Neurology*, 12, 647848. <https://doi.org/10.3389/fneur.2021.647848>
- Ter Telgte, A., Van Leijsen, E. M. C., Wiegertjes, K., Klijn, C. J. M., Tuladhar, A. M., & De Leeuw, F. E. (2018). Cerebral small vessel disease: From a focal to a global perspective. *Nature Reviews Neurology*, 14, 387–398. <https://doi.org/10.1038/s41582-018-0014-y>
- Tuladhar, A. M., Lawrence, A., Norris, D. G., Barrick, T. R., Markus, H. S., & de Leeuw, F. E. (2017). Disruption of rich club organisation in cerebral small vessel disease. *Human Brain Mapping*, 38, 1751–1766. <https://doi.org/10.1002/hbm.23479>
- Tuladhar, A. M., Reid, A. T., Shumskaya, E., De Laat, K. F., Van Norden, A. G. W., Van Dijk, E. J., Norris, D. G., & De Leeuw, F. E. (2015). Relationship between white matter hyperintensities, cortical thickness, and cognition. *Stroke*, 46, 425–432. <https://doi.org/10.1161/STROKEAHA.114.007146>
- Tuladhar, A. M., van Dijk, E., Zwiers, M. P., van Norden, A. G. W., de Laat, K. F., Shumskaya, E., Norris, D. G., & de Leeuw, F. E. (2016). Structural network connectivity and cognition in cerebral small vessel disease. *Human Brain Mapping*, 37, 300–310. <https://doi.org/10.1002/hbm.23032>
- Tullberg, M., Fletcher, E., DeCarli, C., Mungas, D., Reed, B. R., Harvey, D. J., Weiner, M. W., Chui, H. C., & Jagust, W. J. (2004). White matter lesions impair frontal lobe function regardless of their location. *Neurology*, 63, 246–253. <https://doi.org/10.1212/01.WNL.0000130530.55104.B5>
- Wang, Z. (2012). Improving cerebral blood flow quantification for arterial spin labeled perfusion MRI by removing residual motion artifacts and global signal fluctuations. *Magnetic Resonance Imaging*, 30, 1409–1415. <https://doi.org/10.1016/j.mri.2012.05.004>
- Wardlaw, J. M., Smith, C., & Dichgans, M. (2019). Small vessel disease: Mechanisms and clinical implications. *The Lancet Neurology*, 18, 684–696.

- Wardlaw, J. M., Smith, E. E., Biessels, G. J., Cordonnier, C., Fazekas, F., Frayne, R., Lindley, R. I., O'Brien, J. T., Barkhof, F., Benavente, O. R., Black, S. E., Brayne, C., Breteler, M., Chabriat, H., DeCarli, C., de Leeuw, F. E., Doubal, F., Duering, M., Fox, N. C., ... Dichgans, M. (2013). Neuroimaging standards for research into small vessel disease and its contribution to ageing and neurodegeneration. *The Lancet Neurology*, *12*, 822–838.
- Watts, D. J., & Strogatz, S. H. (1998). Collective dynamics of “small-world” networks. *Nature*, *393*, 440–442. <https://doi.org/10.1038/30918>
- Wee, C. Y., Yap, P. T., & Shen, D. (2013). Prediction of Alzheimer's disease and mild cognitive impairment using cortical morphological patterns. *Human Brain Mapping*, *34*(12), 3411–3425. <https://doi.org/10.1002/hbm.22156>
- Wen, W., Sachdev, P. S., Li, J. J., Chen, X., & Anstey, K. J. (2009). White matter hyperintensities in the forties: Their prevalence and topography in an epidemiological sample aged 44–48. *Human Brain Mapping*, *30*, 1155–1167. <https://doi.org/10.1002/hbm.20586>
- Xu, X., Lau, K. K., Wong, Y. K., Mak, H. K. F., & Hui, E. S. (2018). The effect of the total small vessel disease burden on the structural brain network. *Scientific Reports*, *8*(1), 7442. <https://doi.org/10.1038/s41598-018-25917-4>
- Zalesky, A., Fornito, A., Harding, I. H., Cocchi, L., Yücel, M., Pantelis, C., & Bullmore, E. T. (2010). Whole-brain anatomical networks: Does the choice of nodes matter? *NeuroImage*, *50*(3), 970–983. <https://doi.org/10.1016/j.neuroimage.2009.12.027>

SUPPORTING INFORMATION

Additional supporting information may be found in the online version of the article at the publisher's website.

How to cite this article: Kim, W. S. H., Luciw, N. J., Atwi, S., Shirzadi, Z., Dolui, S., Detre, J. A., Nasrallah, I. M., Swardfager, W., Bryan, R. N., Launer, L. J., & MacIntosh, B. J. (2022). Associations of white matter hyperintensities with networks of gray matter blood flow and volume in midlife adults: A coronary artery risk development in young adults magnetic resonance imaging substudy. *Human Brain Mapping*, *43*(12), 3680–3693. <https://doi.org/10.1002/hbm.25876>